



# Isotopic signals in fracture-filling calcite showing anaerobic oxidation of methane in a granitic basement

Takashi Mizuno<sup>a,\*</sup>, Yohey Suzuki<sup>b</sup>, Antoni Edward Milodowski<sup>c</sup>, Teruki Iwatsuki<sup>d</sup>

<sup>a</sup> Geological Disposal Research and Development Department, Japan Atomic Energy Agency, Tokai-Mura, Ibaraki, Japan

<sup>b</sup> Department of Earth and Planetary Science, The University of Tokyo, Bunkyo, Japan

<sup>c</sup> British Geological Survey, Keyworth, Nottinghamshire, UK

<sup>d</sup> Horonobe Underground Research Center, Japan Atomic Energy Agency, Horonobe-cho, Hokkaido, Japan

## ARTICLE INFO

Editorial handling by: Dr F Chabaux

### Keywords:

Fracture-filling calcite  
Anaerobic methane oxidation  
Granitic groundwater  
Paleohydrogeology

## ABSTRACT

Understanding the long-term redox conditions and the related carbon cycle in groundwater is essential for long-term safety assessment because they affect the performance of barrier systems and radionuclide transport in geological disposal. However, it is difficult to identify those long-term changes directly. To help understand this, we conducted a paleohydrogeological study on calcite mineralization associated with fracture-controlled groundwater flow-paths in the Toki Granite in central Japan, focusing on its carbon and oxygen stable isotope characteristics. Previous studies revealed four generations of fracture-filling calcite in the Toki Granite. Therefore, we conducted isotopic analysis on both bulk samples of calcite and spatially-resolved microsamples of discrete generations of calcite within zoned crystals. The  $\delta^{18}\text{O}_{\text{VPDB}}$  of calcite ranging between  $-32.7\text{‰}$  to  $-0.59\text{‰}$  revealed that the groundwater that precipitated the calcite was derived from various origins over the geological history of the area, including early hydrothermal fluids associated with the late-stage cooling of the granite (less than  $-17.2\text{‰}$ ); freshwater invasion from the surface following regional uplift ( $-18.5\text{‰}$  to  $-8.3\text{‰}$ ), and; seawater that penetrated during periods of marine transgression ( $-8.7\text{‰}$  to  $-0.3\text{‰}$ ). The range in  $\delta^{13}\text{C}_{\text{VPDB}}$  values ( $-56.5\text{‰}$  to  $+6.0\text{‰}$ ) was wider than the isotopic range of dissolved inorganic carbon (DIC) that originated from hydrothermal, meteoric, and seawater sources ( $-25\text{‰}$  to  $+2\text{‰}$ ). Calcite with low  $\delta^{13}\text{C}_{\text{VPDB}}$  values less than  $-25\text{‰}$  is believed to have precipitated from groundwater with DIC that was provided by anaerobic oxidation of methane (AOM), whereas calcite with  $\delta^{13}\text{C}_{\text{VPDB}}$  higher than  $+2\text{‰}$  is believed to have precipitated from groundwater containing  $^{13}\text{C}$ -enriched DIC as a carbon source derived during methanogenesis. These processes influencing the formation of calcite mineralization in the Toki Granite are comparable to those at other crystalline rock sites in European countries. The AOM calcite and calcite associated with methanogenesis in the Toki Granite precipitated during the transition of the groundwater origin from meteoric to seawater. Understanding these redox processes and the related carbon cycle in granitic groundwater can provide important insights into processes relevant to assessing the long-term evolution of geoenvironmental systems.

## 1. Introduction

The chemical composition, pH, and redox conditions of groundwater are essential factors that must be considered in the long-term safety assessment for geological disposal of high-level radioactive waste (IAEA, 2012; OECD/NEA, 2013; Posiva Oy, 2012; SKB, 2011). Therefore, understanding the long-term evolution and the drivers of change in groundwater chemistry over geological time scales relevant to that considered in safety assessment (i.e. typically  $10^5$ – $10^6$  years) is important (Blyth et al., 2009). The potentially transient nature of groundwater

chemistry makes it difficult to determine how it has changed over such long periods directly from the present-day groundwater composition alone. However, a paleohydrogeological approach can be employed, which utilizes secondary minerals that may preserve a more continuous record of information about past groundwater chemistry (e.g., Bath et al., 2000; Degnan et al., 2005; Drake and Tullborg, 2009; Milodowski et al., 2018).

Calcite is a particularly useful mineral for paleohydrogeological studies because it forms under a variety of conditions, and can preserve information on long-term changes in the hydrochemical properties of

\* Corresponding author.

E-mail address: [mizuno.takashi@jaea.go.jp](mailto:mizuno.takashi@jaea.go.jp) (T. Mizuno).

<https://doi.org/10.1016/j.apgeochem.2023.105571>

Received 10 October 2022; Received in revised form 6 January 2023; Accepted 12 January 2023

Available online 20 January 2023

0883-2927/© 2023 The Authors. Published by Elsevier Ltd. This is an open access article under the CC BY-NC-ND license (<http://creativecommons.org/licenses/by-nc-nd/4.0/>).

the paleo-groundwaters recorded within; (i) chemical and isotopic composition variations in crystal growth zones; (ii) fluid inclusions, and; (iii) chemically-influenced crystal growth morphology; (Drake et al., 2012, 2015; Iwatsuki et al., 2002; Milodowski et al., 2005; Sahlstedt et al., 2013, 2016; Tullborg et al., 2008). The stable isotope composition of calcite is one of the key features for understanding the mechanisms that influenced groundwater chemistry in the past.  $\delta^{18}\text{O}$  in calcite can be a primary indicator of the origin of groundwater and temperature at the time of precipitation, whereas  $\delta^{13}\text{C}$  reflects the carbon isotopic composition of the DIC pool in groundwater (e.g., Clark and Fritz, 1997). Recent studies have revealed the presence of calcite derived from carbon supplied to a DIC pool by microbial anaerobic oxidation of methane (AOM), in crystalline rocks deep in the terrestrial subsurface that are candidates as potential host rocks for geological disposal (Drake et al., 2015, 2018; Sahlstedt et al., 2016). AOM provides a groundwater DIC pool with carbon that contains very low  $\delta^{13}\text{C}$ ; consequently, the  $\delta^{13}\text{C}$  of the calcite precipitating from this groundwater is also very low (e.g., Drake et al., 2015; Sahlstedt et al., 2016). The metabolic activities of subsurface microorganisms are known to influence the redox conditions of groundwater (Hallbeck and Pedersen, 2008). Microbial communities in Olkiluoto, Finland, have been shown to be active in reducing nitrate, iron, and sulfate (e.g., Bomberg et al., 2015). AOM is known to reduce nitrate ( $\text{NO}_3^-$ ), nitrite ( $\text{NO}_2^-$ ), sulfate ( $\text{SO}_4^{2-}$ ), iron ( $\text{Fe}^{3+}$ ), and manganese ( $\text{Mn}^{4+}$ ), which are major aqueous redox-buffering species (Stumm and Morgan, 1996). From the viewpoint of safety assessment for geological disposal of radioactive waste, it is important to understand the contribution of AOM to DIC, and its relationship to changes in groundwater chemistry due to redox reactions. However, few studies have been conducted on AOM in deep groundwater systems of crystalline rocks.

Previous studies in the Mizunami area, the target area of this study, have focused on microorganisms in granite groundwater (Fukuda et al., 2010; Ino et al., 2018; Suzuki et al., 2014), but previous paleohydrogeological studies based on the fracture-filling calcite in the Toki Granite (Iwatsuki et al., 2002, 2010; Mizuno et al., 2010, 2022) have not considered chemical processes involving microorganisms as well as AOM. Therefore, the present study aims to understand the contribution of AOM and associated processes to DIC in the long-term hydrochemical evolution by focusing on newly obtained stable isotopic data, combined together with existing data from previous studies (Iwatsuki et al., 2002; Mizuno et al., 2010), obtained from fracture-filling calcite in the Toki Granite in the Mizunami area.

## 2. Background information

The Mizunami area is located in Gifu Prefecture in central Japan, approximately 300 km west of Tokyo (Fig. 1a). The Mizunami Underground Research Laboratory (MIU) is a purpose-built generic underground research facility for developing technologies for geological disposal in crystalline rocks. The MIU had two 500m deep vertical shafts with horizontal tunnels that connected the two shafts (Fig. 1b). They were backfilled as the research and development project was completed. (Fig. 1b). The basement geology of this area comprises the Cretaceous Toki Granite, which is overlain by the sedimentary rocks of the Paleogene Mizunami Group and Quaternary Tokai Group (Sasao, 2013) (Fig. 1a). Previous thermochronological studies focusing on the Toki Granite revealed that the granite was emplaced during the Cretaceous (Shibata and Ishihara, 1979). The zircon and apatite fission-track dating reveal the cooling history of 190 °C–390 °C from 75.6 Ma to 54.6 Ma; 90 °C–120 °C from 49.5 Ma to 37.1 Ma in the granite (Table 1) (Yuguchi et al., 2019). Mineralogical studies of fracture fillings (Ishibashi et al., 2016) indicate that no subsequent granite-related hydrothermal activity occurred. It can be inferred that after 35 Ma, temperature conditions evolved along a geothermal gradient, similar to that of the present day (Table 1). Based on the fracture frequency, the Toki granite can be divided into the upper highly fractured domain (UHFD) with a high fracture frequency, and the lower sparsely fractured domain (LSFD) with a low fracture frequency (Tsuruta et al., 2013). The boundary depth is not constant over this area but is approximately several hundred meters deep (Iwatsuki et al., 2010; Yuguchi et al., 2021). The depositional environment of the Mizunami Group varied over time. In its early stages, fluvial-lacustrine arenaceous sediments of the organic-rich Toki lignite-bearing Formation (27–20 Ma) (Iwatsuki et al., 2004), and the Hongo Formation (19–18 Ma) were deposited (Hiroki and Matsumoto, 1999; Sasao et al., 2006). They were followed by marine transgression that resulted in the deposition of the Akeyo Formation (17 Ma) in a shallow marine environment, which was interrupted by a period of regression, erosion, and non-deposition (17–15 Ma) before the renewed marine deposition of the Oidawara Formation (15 Ma) (Sasao et al., 2006). Subsequently, the lacustrine Tokai Group was deposited between 12 and 1.5 Ma, and then the Mizunami area has been uplifted since 1.5 Ma (Table 1) (Sasao et al., 2006).

The present-day groundwater is dominated by  $\text{Na-HCO}_3$ -type groundwater of meteoric origin over much of the area (Iwatsuki and Yoshida, 1999). However,  $\text{NaCl}$ -type groundwater is present in the southern part, associated with the Tsukiyoshi Fault, and was

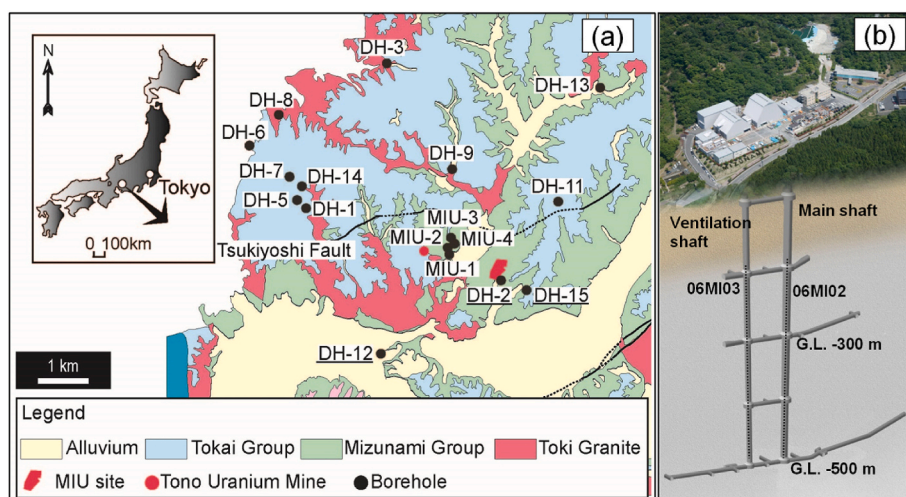


Fig. 1. Overview of the study area and sampling location. a) Geological Map of the Mizunami area and location of boreholes in which fracture filling calcite was sampled. b) Overview of the Mizunami Underground facility (MIU). Two boreholes shown by the dotted line were drilled from the bottom of the Main and Ventilation shaft as pilot boreholes of the shafts.

**Table 1**

The geological history of the Mizunami area and precipitation sequence of fracture-filling calcite (modified after Mizuno et al. (2022)).

Timescale	Geological event	Origin of groundwaters in the basement granite	Salinity and Temperature of the groundwaters	Calcite generation (mineralogical characteristics)
c.75Ma	Toki Granite intrusion			
75.6–54.6 Ma	brittle faulting and subsequent geothermal event	Hydrothermal fluid	Salinity is unknown [190 °C–390 °C]	Calcite I (typically anhedral, moderate to bright luminescence)
49.5–37.1 Ma	Cooling with uplift	Warm hydrothermal fluid	Salinity is unknown [60 °C–120 °C]	
35–27 Ma	uplift and subareal exposure and erosion (Deep weathering of Toki granite)	Meteoric [Freshwater]	Salinity in fluid inclusions hosted by fracture-filling calcite is varied with 0.47–4.53 (wt.% NaCl Eq.). [ $< 90$ °C]	Calcite II (equant to slightly c-axis elongated form, moderate to bright luminescence) & Calcite III (distinctly elongated along the c-axis form, generally dull but locally and variably bright luminescence)
27–20 Ma?	Deposition of the Toki Lignite-bearing Fm	Meteoric + Riverine [Freshwater]		
19–18 Ma?	Deposition of the Hongo Formation			
c.17Ma	Deposition of Akeyo Formation	Seawater invasion [Saline]		
17–15 Ma	Unconformity	Possible meteoric invasion? [? Freshwater]		
c. 15 Ma	Deposition of the Oidawara Formation	Seawater invasion [Saline]		
15–12 Ma	Major unconformity between Mizunami and Tokai Group	Meteoric invasion [Freshwater]		
12–1.5 Ma	Deposition of the Tokai Group sediments	Meteoric + Lacustrine [Freshwater recharge]	Diluted groundwater [ $< 90$ °C]	Calcite IV (microporous or gel-like “globular” deposits or micro-crystalline coatings on the corroded surfaces of Calcite III, relatively bright luminescence)
c. 1.5-present	Base-level change due to regional uplift	Meteoric invasion ongoing [Freshwater recharge]		

**Table 2**

$\delta^{13}\text{C}$  and  $\delta^{18}\text{O}$  data of spatially-resolved calcite microsamples shown in Fig. 3. Microsamples taken from the regions shown in Fig. 3 are mixed before analysis. Therefore, the analytical values shown in the table are averages for each region. Estimated isotopic values in groundwater from which calcite precipitated are calculated based on Eq. (2), Eq. (3), Eq. (4), and Eq. (5), as well as the method described in section 4.1.

Calcite Generation	Sub-sample	Measured isotopic values in calcite		Estimated isotopic values in groundwater from which calcite precipitated	
		$\delta^{13}\text{C}_{\text{VPDB}}$ (‰)	$\delta^{18}\text{O}_{\text{VPDB}}$ (‰)	$\delta^{13}\text{C}_{\text{VPDB}}$ (‰)	$\delta^{18}\text{O}_{\text{VSMOW}}$ (‰)
II	1	–56.0	–11.4	–59.3 ~	–11.2 ~
	2	–54.7	–11.5	–56.5	–2.7
	3	–55.4	–11.4		
	4	–56.5	–11.5		
III	5	0.0	–7.0	–6.6 ~	–7.6 ~
	6	–3.8	–7.9	–1.8	+1.7

encountered in the underlined boreholes and the MIU site shown in Fig. 1 (Iwatsuki et al., 2005). The residence time of granitic groundwater in and around the MIU is estimated to be over 50,000 years at depths of around 600 m below the surface, below which  $^{14}\text{C}$  is no longer detectable (Iwatsuki et al., 2005). The previous paleo-hydrogeological studies focused on the fracture-filling calcite in the Toki Granite and have revealed that past groundwaters originated from the circulation of early hydrothermal fluids, as well as from seawater, meteoric water, or river and lake water introduced during episodes of marine transgression and regression, and subaerial uplift (Iwatsuki et al., 2002, 2010; Mizuno et al., 2010, 2022). The paragenetic sequence of fracture-filling calcite mineralization could be divided into four stages, referred to as Calcite I to IV (from oldest to youngest), that reflect the changes in groundwater chemistry (Mizuno et al., 2022). Detailed petrographic analyses, together with fluid inclusion microthermometry, stable (C, O) isotope, and chemical composition data of fracture-filling calcite in the earlier studies (Mizuno et al., 2010, 2022), enable the mineralization to be correlated with the geological evolution of the Mizunami area. (Table 1).

Two types of methane with markedly different  $\delta^{13}\text{C}$  signatures have also been identified in the present-day granitic groundwaters. One is the methane supplied from the deeper part of the sequence through fractures, with  $\delta^{13}\text{C}_{\text{VPDB}}$  in the range of  $-21.0\text{‰} \sim -45.3\text{‰}$ , that has been identified in and around the MIU site (Iwatsuki et al., 2005; Kurosawa et al., 2010; Niwa et al., 2021; Suzuki et al., 2014). The concentration of this methane is depth-dependent, with the highest concentration detected to date being 688  $\mu\text{M}$  at a depth of 945 m below the surface (Iwatsuki et al., 2005). The origin of the methane is thought to be thermogenic based on the range of isotopic compositions (Ino et al., 2018; Iwatsuki et al., 2005). The other methane type is identified from the unconformity between the Toki Granite and the overlying sedimentary rocks at the Tono uranium mine, located about 2 km west of the MIU (Fig. 1). The  $\delta^{13}\text{C}_{\text{VPDB}}$  of this methane is  $-97.1\text{‰}$  and is considered to be microbial methane (Mills et al., 2010). Genome analysis of microorganisms sampled from present-day groundwater and laboratory experiments indicate that AOM associated with sulfate reduction may occur in the UHFD by ANME-2d and that microbial methanogenesis may occur in the LSFd (Ino et al., 2018). These hydrochemical baseline conditions are summarized in Table S1.

### 3. Approach

#### 3.1. Sampling

The calcite samples for carbon and oxygen isotopic analysis were collected from the cores recovered from several boreholes drilled in the Toki granite. These included: DH-15, a deep vertical borehole drilled from the surface, and; 06MI03, one of the vertical pilot boreholes drilled from within the shafts during the MIU construction (Fig. 1). Eight samples were collected from DH-15 and six samples from 06MI03. One sample, collected from DH-15, where sufficient sample volume was obtained, was specifically prepared as a polished block for subsequent micro-sampling, and was petrographically examined by cathodoluminescence (CL) microscopy using a Technosyn Model 8200 Mark II cold cathodoluminoscope stage mounted on a Nikon optical microscope.

Microsamples for oxygen and carbon isotope analysis were obtained

from single calcite growth zones of  $\sim 100 \mu\text{m}$  wide using an optical microscope-mounted tungsten carbide microdrill (New Wave Research Inc., MicroMill). The microsampling locations of discrete calcite zones and generations were guided by the CL images of the polished block, and the drill depth was set from 50 to 200  $\mu\text{m}$  to avoid contamination. The other calcite samples were treated as bulk samples for analysis for the oxygen and carbon isotopic composition. Existing data (Iwatsuki et al., 2002; Mizuno et al., 2010) were summarized and used together with the new data obtained in the present study.

### 3.2. Method

The carbon and oxygen isotopic analysis of calcite was performed using a VG Isocarb and Optima mass spectrometer (Micromass UK Ltd.). Small amounts of each powdered-carbonate mineral sample were converted to  $\text{CO}_2$  gas by allowing them to react with 100% phosphoric acid in a vacuum line. The isotope values ( $\delta^{13}\text{C}$  and  $\delta^{18}\text{O}$ ) were presented in per mil (‰) deviations of the isotopic ratios ( $^{13}\text{C}/^{12}\text{C}$  and  $^{18}\text{O}/^{16}\text{O}$ ), which were calculated relative to the Vienna Pee Dee Belemnite international standard (VPDB). This standard referred back to the original PDB standard, which was calibrated against the NBS-19 standards and analyzed together with the samples. The analytical reproducibility values of NBS-19 were  $\delta^{18}\text{O}_{\text{VPDB}} = \pm 0.05\text{‰}$  ( $1\sigma$ ,  $n = 21$ ) and  $\delta^{13}\text{C}_{\text{VPDB}} = \pm 0.03\text{‰}$  ( $1\sigma$ ,  $n = 21$ ), and those of the laboratory standard calcite were  $\delta^{18}\text{O}_{\text{VPDB}} = \pm 0.05\text{‰}$  ( $1\sigma$ ,  $n = 6$ ) and  $\delta^{13}\text{C}_{\text{VPDB}} = \pm 0.03\text{‰}$  ( $1\sigma$ ,  $n = 6$ ). In this study, the isotopic compositions of calcite, both  $\delta^{13}\text{C}$  and  $\delta^{18}\text{O}$ , are presented as VPDB-standard values. However,  $\delta^{18}\text{O}$  in groundwater was based on the Standard Mean Ocean Water (VSMOW)-standard value. The conversion between  $\delta^{18}\text{O}_{\text{VPDB}}$  and  $\delta^{18}\text{O}_{\text{VSMOW}}$  followed Equation (1) (Gonfiantini, 1984).

$$\delta^{18}\text{O}_{\text{VSMOW}} = 1.03086 \cdot \delta^{18}\text{O}_{\text{VPDB}} + 30.86 \quad (1)$$

## 4. Result and discussion

### 4.1. Origin of groundwater from which calcite has been precipitated based on bulk-analysis

The result of bulk-analysis of fracture-filling calcite in this study shows  $\delta^{13}\text{C}_{\text{VPDB}}$  ranging from  $-42.1\text{‰}$  to  $-7.0\text{‰}$  and  $\delta^{18}\text{O}_{\text{VPDB}}$  ranging from  $-14.2\text{‰}$  to  $-3.3\text{‰}$  (open symbols in Fig. 2, Table S2). Combining these results with those of bulk-analysis in previous studies (Iwatsuki et al., 2002; Mizuno et al., 2010), the ranges of  $\delta^{13}\text{C}_{\text{VPDB}}$  and  $\delta^{18}\text{O}_{\text{VPDB}}$  were  $-42.1\text{‰}$  to  $+6.0\text{‰}$  and  $-32.4\text{‰}$  to  $+0.59\text{‰}$ , respectively (Fig. 2). This wide distribution of isotopic compositions in the calcites reflects the changes in the origin of groundwater distributed in the Mizunami area in the past (Iwatsuki et al., 2002, 2010; Mizuno et al., 2010). Although previous studies have compared the isotopic composition of the fracture-filling calcite with that of inferred paleo-groundwaters (Iwatsuki et al., 2002; Mizuno et al., 2010, 2022), in this study, the temperature effect during isotope fractionation was also taken into account and re-examined.

The isotopic fractionation of carbon was calculated, according to the method of Blyth et al. (2009), using the isotopic fractionation factor obtained from Equation (2) (Blyth et al., 2009), (3) (Mook et al., 1974), and (4) (Bottinga, 1968).

$$10^3 \cdot \ln \alpha_{\text{HCO}_3\text{-calcite}} = 10^3 \cdot \ln \alpha_{\text{HCO}_3\text{-CO}_2} + 10^3 \cdot \ln \alpha_{\text{CO}_2\text{-calcite}} \quad (2)$$

$$10^3 \cdot \ln \alpha_{\text{HCO}_3\text{-CO}_2} = 9.552 \cdot (10^3 \cdot \text{T}^{-1}) - 24.10 \quad (3)$$

$$10^3 \cdot \ln \alpha_{\text{CO}_2\text{-calcite}} = 2.9880 \cdot (10^6 \cdot \text{T}^{-2}) + 7.663 \cdot (10^3 \cdot \text{T}^{-1}) - 2.4612 \quad (4)$$

[where T is the temperature in Kelvin and  $\alpha$  is the isotopic fractionation factor].

For groundwater of seawater origin, both  $\delta^{13}\text{C}_{\text{VPDB}}$  and  $\delta^{18}\text{O}_{\text{VSMOW}}$

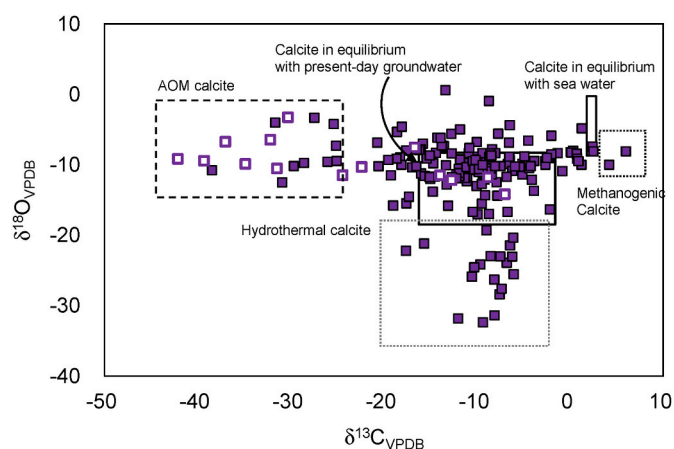


**Fig. 2.** Plot of  $\delta^{13}\text{C}_{\text{VPDB}}$  and  $\delta^{18}\text{O}_{\text{VPDB}}$  of fracture-filling calcite analyzed by bulk analysis. Open symbols show the data newly obtained in this study. The range of “Calcite in equilibrium with present-day groundwater” is estimated from the isotopic data of present-day groundwater (Mizutani et al., 1992; Iwatsuki et al., 2001, 2005; Suzuki et al., 2014). The range of “hydrothermal calcite” is estimated assuming past hydrothermal environment. The “Calcite in equilibrium with sea water” range is referenced to  $\delta^{13}\text{C}_{\text{VPDB}}$  of 0‰ and  $\delta^{18}\text{O}_{\text{VPDB}}$  of 0‰, respectively. Calcite with  $\delta^{13}\text{C}_{\text{VPDB}}$  lower than  $-25\text{‰}$  is considered AOM calcite, and calcite with  $\delta^{13}\text{C}_{\text{VPDB}}$  higher than  $+2.8\text{‰}$  is considered methanogenic calcite. See text for details.

were set to 0‰ as reference values. For groundwater of meteoric origin, the ranges indicated by  $\delta^{13}\text{C}_{\text{VPDB}}$  and  $\delta^{18}\text{O}_{\text{VSMOW}}$  for groundwater of present meteoric origin (unaffected by the disturbances associated with the construction of the MIU) were used as references ( $\delta^{13}\text{C}_{\text{VPDB}}$ :  $-18.0\text{‰} \sim -4.4\text{‰}$ ;  $\delta^{18}\text{O}_{\text{VSMOW}}$ :  $-9.9\text{‰} \sim -8.0\text{‰}$ ) (Iwatsuki et al., 2002, 2005; Mizutani et al., 1992). The  $\delta^{13}\text{C}$  in present-day groundwater exhibits a widely-distributed depth dependence, becoming higher at depth. However, mineral precipitation and microbial reduction are not the cause of the depth dependence but rather it reflects a mixing between DIC with relatively higher  $\delta^{13}\text{C}$  at depth and DIC with lower  $\delta^{13}\text{C}$  at shallower depths.

The oxygen isotopic ratio is calculated using Equation (5) (O’Neil et al., 1969).

$$10^3 \cdot \ln \alpha_{\text{oxy}} = 2.78 \cdot (10^6 \cdot \text{T}^{-2}) - 3.39 \quad (5)$$

Because isotopic fractionation factors for both carbon and oxygen are temperature dependent, it is necessary to estimate the paleo-temperature at which calcite precipitation occurred. Since it was impossible to determine each sample’s precipitation temperature directly, the temperature conditions were calculated from the geothermal gradient and burial depth of the Toki Granite. Based on the results of borehole logging, the geothermal gradient was assumed to be ca.  $3 \text{ }^\circ\text{C}/100\text{m}$  (Saegusa and Matsuoka, 2011). The Toki Granite was at its deepest following emplacement, during the deposition of the Tokai Formation, and the total maximum thickness of the Mizunami and Tokai groups is 575 m (Sasao et al., 2005). Since the Toki Granite is exposed at the surface in some places, it is assumed that the maximum depth was about 575 m deeper than at present. The maximum burial depth at the deepest point sampled in this study (which is ca. 900 m below the unconformity) would have been about 1475 m below ground surface. Assuming a surface temperature of  $15 \text{ }^\circ\text{C}$ , based on the present-day geothermal gradient, it is estimated to have ranged from  $15 \text{ }^\circ\text{C}$  to  $60 \text{ }^\circ\text{C}$ . Although this estimation involves uncertainty, the temperature conditions were assumed to be within this range for paleo-groundwaters of meteoric water and seawater origin. This estimate is consistent with the occurrence of fluid inclusions (identified previously in Calcite II and Calcite III) as being monophasic liquid inclusions (Mizuno et al., 2010) that generally form under low-temperature ( $< 80 \text{ }^\circ\text{C}$ ) conditions (Gill

et al., 2014; Roedder, 1984).

The isotopic compositions of calcites expected to precipitate in equilibrium from each type of groundwater were calculated using Equations (2) to (5). The predicted  $\delta^{13}\text{C}_{\text{VPDB}}$  and  $\delta^{18}\text{O}_{\text{VPDB}}$  of calcite precipitated from groundwater of seawater origin ranged from 1.8‰ to 2.8‰ and from -8.7‰ to -0.3‰, respectively. The predicted  $\delta^{13}\text{C}_{\text{VPDB}}$  and  $\delta^{18}\text{O}_{\text{VPDB}}$  of calcite precipitated from groundwater of meteoric origin ranged from -16.2‰ to -1.6‰ and -18.5‰ to -8.3‰, respectively (Table S3).

Regarding the oxygen isotopic ratio of calcite precipitated from hydrothermal fluids, previous studies assumed that the  $\delta^{18}\text{O}_{\text{VSMOW}}$  of paleo-groundwaters in the Mizunami area was 0 to -10‰ (which is the range of meteoric water and seawater) and noted that temperatures above 230 °C are required for calcite precipitation with  $\delta^{18}\text{O}_{\text{VPDB}}$  of -32.5‰ (Iwatsuki et al., 2002). However, it is known that  $\delta^{18}\text{O}$  in hydrothermal water becomes higher due to intense water-rock interaction (e.g., Clark and Fritz, 1997). For example,  $\delta^{18}\text{O}_{\text{VSMOW}}$  is +8‰ in the Arima hot spring water in Japan (Sakai and Matsubaya, 1974). Assuming the temperature at which the fractures formed in the Toki Granite was 300 °C (Yamasaki et al., 2013), then if  $\delta^{18}\text{O}_{\text{VSMOW}}$  of the paleo-fluids in the associated hydrothermal circulation system is assumed to have been +8‰, the  $\delta^{18}\text{O}_{\text{VPDB}}$  of calcite in equilibrium with this fluid is calculated to be -17.2‰ based on Equation (4). Thus, calcite with  $\delta^{18}\text{O}_{\text{VPDB}}$  lower than -17.2‰ may be assumed to have precipitated in a hydrothermal environment (Table S3).

Fig. 2 summarises these results and compares them with the  $\delta^{18}\text{O}$  of fracture-filling calcites analyzed from the Toki Granite. This shows that the calcite mineralization encountered in the Toki Granite can be explained by precipitation from a variety of groundwaters of seawater, freshwater, and hydrothermal origin, or their mixtures, over time. However, the  $\delta^{13}\text{C}$  of many of the calcite samples are far lighter than expected, and fall well outside the predicted compositional ranges calculated above. DIC in present-day granitic groundwater is supplied by soil  $\text{CO}_2$  and the decomposition of organic matter in the overlying sedimentary rocks (Iwatsuki et al., 2001, 2005). The  $\delta^{13}\text{C}_{\text{VPDB}}$  values of soil  $\text{CO}_2$  and sedimentary organic matter are -20‰ (Iwatsuki et al., 2005) and -25‰ (Iwatsuki et al., 1995; Shikazono and Utada, 1997), respectively. Therefore, calcite with  $\delta^{13}\text{C}_{\text{VPDB}}$  that is lower than -25‰ or higher than +2.8‰ indicates the presence of a different carbon source than soil  $\text{CO}_2$  or carbon supplied by the breakdown of organic matters or DIC in seawater. The very low  $\delta^{13}\text{C}$  values found in some of the fracture-filling calcites in the Toki Granite are close to the range of values observed in methane-derived authigenic carbonate deposits formed by AOM at seafloor methane seepage sites (e.g. Douglas et al., 2017; Judd et al., 2019; Judd and Hovland, 2007; Schoell, 1980). Because no other carbon source with  $\delta^{13}\text{C}_{\text{VPDB}}$  lower than -25‰ is observed in the study area except methane, the calcite with significantly

low  $\delta^{13}\text{C}_{\text{VPDB}}$  observed in this study most likely precipitated from DIC supplied by AOM as a carbon source. However, calcite with  $\delta^{13}\text{C}_{\text{VPDB}}$  values higher than +2.8‰ also exists, which suggests that methanogenesis may have shifted the isotopic composition of residual DIC to a relative  $^{13}\text{C}$  enrichment (e.g. Drake et al., 2017; Sahlstedt et al., 2016; Sandström and Tullborg, 2009).

#### 4.2. Spatiotemporal distribution of AOM calcite as shown by micro-analysis

The results of the micro-analysis of the DH-15 samples newly conducted in the study were as follows (Fig. 3, Table S4):

Calcite II (3 regions)  $\delta^{13}\text{C}_{\text{VPDB}}$ : -56.5‰ ~ -54.7‰;  $\delta^{18}\text{O}_{\text{VPDB}}$ : -11.5‰ ~ -11.4‰

Calcite III (2 regions)  $\delta^{13}\text{C}_{\text{VPDB}}$ : -3.8‰-0.0‰;  $\delta^{18}\text{O}_{\text{VPDB}}$ : -7.9‰ ~ -7.0‰

This sample showing the most negative  $\delta^{13}\text{C}_{\text{VPDB}}$  is dominated by fracture surfaces lined by Calcite II mineralization varying in thickness from 1 mm to several millimeters. It also displays overgrowths, approximately 1 mm thick, of later c-axis elongated crystals of Calcite III (differentiated by its slightly darker CL) nucleated on top of Calcite II (Fig. 3). Calcite II and Calcite III are clearly different in both their isotopic composition and CL characteristics (Fig. 3, Table 2), reflecting discontinuous precipitation from groundwaters with different hydrochemical properties. The isotope data has been differentiated in regard to the generation of calcite dominating in each of the samples, as distinguished on the basis of CL petrography (cf. Mizuno et al., 2022). The analysis result from this sample indicates that AOM was operating during Calcite II precipitation. Since the precipitation of Calcite II is considered to have occurred following the deposition of the Toki Lignite-bearing Formation, it can be inferred that Calcite II was potentially formed in a freshwater environment. However, the  $\delta^{18}\text{O}_{\text{VSMOW}}$  of groundwater from which the calcite precipitated is estimated to be -11.2‰ to -2.7‰ based on the  $\delta^{18}\text{O}_{\text{VPDB}}$  of Calcite II in the temperature range assumed in section 4.1 (Table 2), indicating that it is difficult to determine the origin of the groundwater as meteoric water or seawater. Although the estimated  $\delta^{13}\text{C}$  of the groundwater from which Calcite III precipitated shows a comparable value with the DIC of seawater,  $\delta^{18}\text{O}$  may differ from the value of seawater (Table 2). These isotopic characteristics suggest that Calcite II and Calcite III precipitated in an environment where groundwater of seawater origin mixed with water of meteoric origin. The microthermometry of fluid inclusions in Calcite II and Calcite III has also revealed that groundwater salinity varied within the range of freshwater to seawater during the precipitation of these calcite generations (Mizuno et al., 2010). Considering the geological history of the area, several episodes of marine transgression and marine

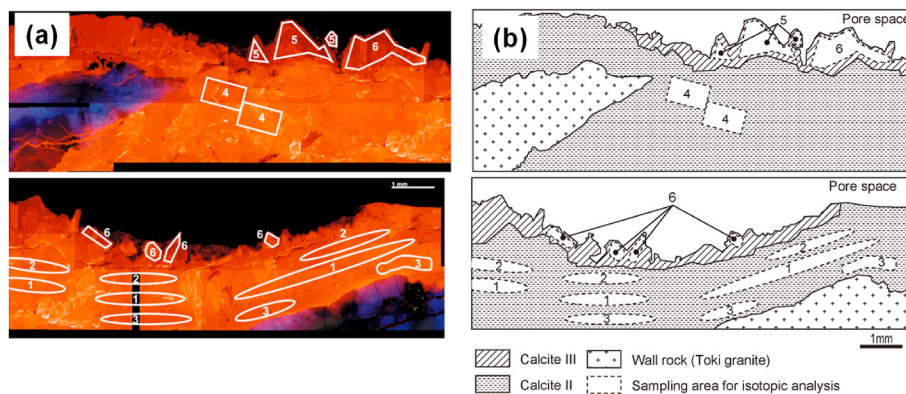


Fig. 3. Location of sampling using micro-drill for isotopic analysis in DH-15 depth of 196.4 m below unconformity (mbu). (a) Cathodoluminescence image and trace of micro-sampling locations; (b) Schematic tracing of the CL image identifying the different calcite generations and trace of micro-sampling location. Isotopic data from each micro-sampling location are shown in Table 2.

regression occurred during this period (Table 1), and would have impacted on groundwater recharge, and are consistent with the hydrochemical changes in the granitic groundwater that can be inferred from the calcite analysis.

The stable isotope data obtained by micro-analyses of the fracture-filling calcites from this present study, together with data from previous studies (Iwatsuki et al., 2002; Mizuno et al., 2010), are presented in Fig. 3 and Table S4. The range of  $\delta^{13}\text{C}_{\text{VPDB}}$  and  $\delta^{18}\text{O}_{\text{VPDB}}$  values observed for each of the four calcite generations is summarized below.

- Calcite I)  $\delta^{13}\text{C}_{\text{VPDB}}$ : from  $-15.3$  to  $-7.5\text{‰}$ ;  $\delta^{18}\text{O}_{\text{VPDB}}$ : from  $-32.7$  to  $-12.1\text{‰}$   
 Calcite II)  $\delta^{13}\text{C}_{\text{VPDB}}$ : from  $-56.5$  to  $-4.6\text{‰}$ ;  $\delta^{18}\text{O}_{\text{VPDB}}$ : from  $-17.02\text{‰}$  to  $-10.3\text{‰}$   
 Calcite III)  $\delta^{13}\text{C}_{\text{VPDB}}$ : from  $-17.99$  to  $5.77\text{‰}$ ;  $\delta^{18}\text{O}_{\text{VPDB}}$ : from  $-11.4$  to  $-2.34\text{‰}$   
 Calcite IV)  $\delta^{13}\text{C}_{\text{VPDB}}$ : from  $-10.6$  to  $-1.7\text{‰}$ ;  $\delta^{18}\text{O}_{\text{VPDB}}$ : from  $-12.7$  to  $-8.2\text{‰}$

The carbon and oxygen isotopic data obtained by micro-analysis were compared to those of calcite predicted to be in equilibrium with present-day groundwater, seawater, and hydrothermal circulation, as described in section 4.1 (Fig. 4). The calcite with around  $-30\text{‰}$  of  $\delta^{18}\text{O}_{\text{VPDB}}$  in Calcite I precipitated in a warm hydrothermal environment before 35Ma. The  $\delta^{18}\text{O}_{\text{VPDB}}$  of the other Calcite I samples are distributed in the range that is in equilibrium with the present-day groundwater. It suggests they precipitated from groundwater with a similar isotopic composition to present-day groundwater (Fig. 4a). In Calcite II, other than the AOM calcite, all but one sample plotted in the range of calcite in equilibrium with present-day groundwater. (Fig. 4b). In contrast, Calcite III contains calcite with  $\delta^{18}\text{O}_{\text{VPDB}}$  values that are close to that of calcite in equilibrium with seawater, which suggests that its precipitation was influenced by groundwater derived from seawater (Fig. 4c). In addition, calcite with more positive  $\delta^{13}\text{C}_{\text{VPDB}}$  than calcite expected to be in equilibrium with seawater can also be identified. Residual  $\text{CO}_2$ , which became  $^{13}\text{C}$ -rich during methanogenesis, can be assumed as the carbon source for calcite with such high  $\delta^{13}\text{C}$  (Drake et al., 2017; Sahlstedt et al.,

2016; Sandström and Tullborg, 2009). Since the maximum  $\delta^{13}\text{C}_{\text{VPDB}}$  was  $+6.0\text{‰}$ , the change of  $\delta^{13}\text{C}$  in the DIC pool is considered limited. The changes in the hydrochemical properties prevailing during Calcite II and Calcite III precipitation may have regulated the occurrence and suspension of AOM and the methane forming process. Both Calcite IV and Calcite II, plot mainly in areas of equilibrium with the present-day groundwater (Fig. 4d). Since Calcite IV is the most recent calcite, it is thought to reflect the isotopic composition of the present-day groundwater.

Fig. 5 shows the  $\delta^{13}\text{C}_{\text{VPDB}}$  of fracture-filling calcite obtained by both bulk- and micro-analysis relative to their depth below the unconformity (mbu). The unconformity is used as a reference because the thickness of the sedimentary layer is not uniform within the study area, and the elevations of the tops of the boreholes vary with the location. The calcite with the most negative  $\delta^{13}\text{C}_{\text{VPDB}}$  ( $-56.5\text{‰}$ ) appears 196.4 m below the unconformity (Fig. 5a). No AOM calcite has been found deeper than 500 mbu (Fig. 5a). In the Toki granite, the UHFD is extends over several hundred meters in the shallow part of the granite (Iwatsuki et al., 2010). The boundary between the UHFD and the LSFD in borehole DH-15 occurs at a depth of 467 mbu (Saegusa and Matsuoka, 2011). Therefore, AOM principally occurred within the UHFD. In contrast, methanogenic calcite more enriched in  $^{13}\text{C}$  is not found at shallower depths (i.e. above  $\sim 200$  mbu) but occurs at the same depth or slightly deeper than AOM calcite (Fig. 5a).

AOM and methanogenesis in present-day groundwater occur at the UHFD and LSFD, respectively (Ino et al., 2018). Therefore, the spatial distribution of past AOM and methanogenesis that can be reconstructed from calcite mineralization is the same as that of their location at present. These suggest that the AOM occurs in shallower, more permeable areas with more microbially-reactive organic components supplied from the shallower parts of the sequence.

#### 4.3. Possible paleo-AOM process in the Mizunami area

The  $\delta^{13}\text{C}_{\text{VPDB}}$  values of methane involved in AOM back-calculated from the lowest  $\delta^{13}\text{C}_{\text{VPDB}}$  of  $-56.5\text{‰}$  recorded from the calcites are estimated to be  $-60.0\text{‰}$  to  $-42.1\text{‰}$  based on Eq. (2) and fractionation

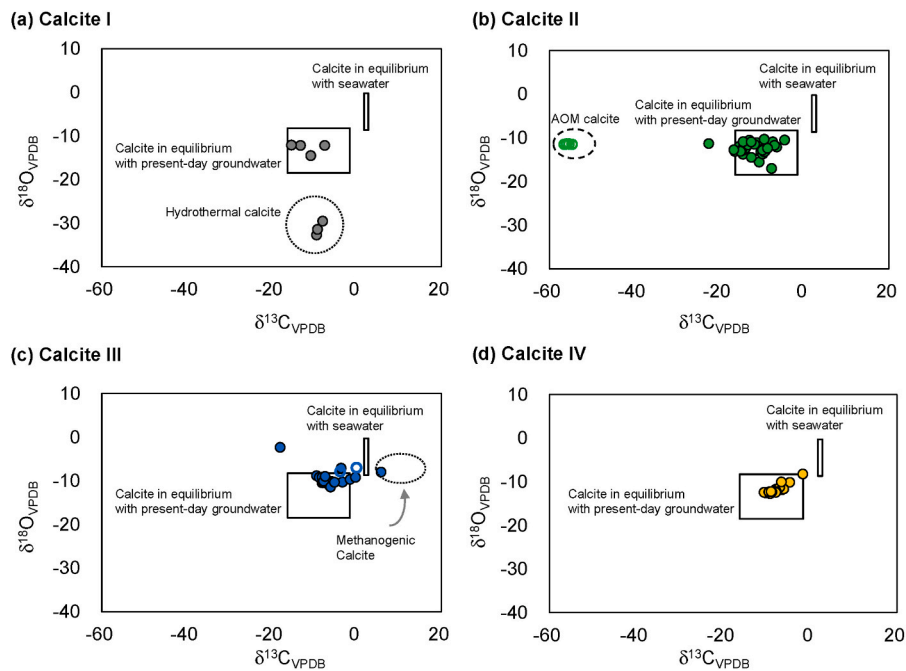
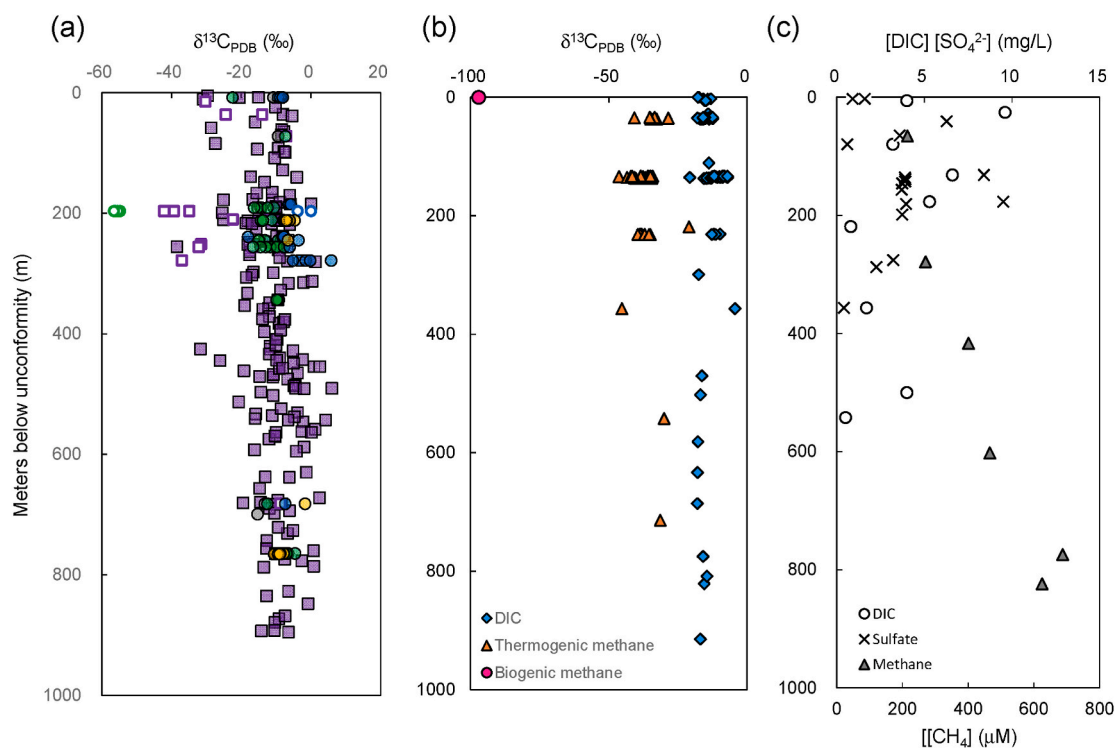


Fig. 4. The plot of  $\delta^{13}\text{C}_{\text{VPDB}}$  and  $\delta^{18}\text{O}_{\text{VPDB}}$  of fracture-filling calcite analyzed by the micro-drilling method in each generation, Calcite I (a), Calcite II (b), Calcite III (c), and Calcite IV (d). Open symbols shown in (b) and (c) indicate the data newly obtained in this study (Table 2). The respective ranges of “Hydrothermal calcite”, “Calcite in equilibrium with present-day groundwater”, “AOM Calcite”, and “Methanogenic Calcite” are based on the same approaches as in Fig. 2.



7

Fig. 5. (a)  $\delta^{13}\text{C}_{\text{VPDB}}$  of the bulk analysis and microanalysis in each generation versus depth; (b)  $\delta^{13}\text{C}_{\text{VPDB}}$  of DIC (Ino et al., 2018; Iwatsuki et al., 2001, 2005; Mizutani et al., 1992; Suzuki et al., 2014), thermogenic methane (Ino et al., 2018; Iwatsuki et al., 2005; Suzuki et al., 2014), and biogenic methane (Mills et al., 2010) in the present-day groundwater; (c) Concentration of DIC, sulfate ion, and methane in present-day groundwater (Iwatsuki et al., 2001, 2005; Mizutani et al., 1992).

factor between  $\text{CH}_4$  and  $\text{CO}_2$  [ $\alpha_{\text{CH}_4\text{-CO}_2}$  = from 1.00838 to 1.022 (Alperin et al., 1988; Chanton et al., 2008)]. The calculated range of  $\delta^{13}\text{C}$  in methane, which represents the potential carbon source for the AOM calcite, is close to the  $\delta^{13}\text{C}$  value of the present-day thermogenic methane ( $\delta^{13}\text{C}_{\text{VPDB}}$  is from  $-46.3\text{‰}$  to  $-21.0\text{‰}$ ) (Ino et al., 2018; Iwatsuki et al., 2005) (Fig. 5b). Because the fracture network in the Toki granite was formed soon after the granite emplacement (Ishibashi et al., 2016), methane profiles in the past may have been similar to those at present (Fig. 5c). The present microbial methane is produced by  $\text{CO}_2$  reduction (Mills et al., 2010), and shows more negative  $\delta^{13}\text{C}$  ( $\delta^{13}\text{C}_{\text{VPDB}} = -97\text{‰}$ ). However, methane with higher  $\delta^{13}\text{C}$  ( $\delta^{13}\text{C}_{\text{VPDB}}: -65\text{‰}$  to  $-50\text{‰}$ ) would be supplied when methanogenesis occurs by the acetolysis pathway in a freshwater environment with low sulfate ion concentrations (Kuivila et al., 1989; Phelps and Zeikus, 1985; Whiticar et al., 1986). A recent comprehensive review of the isotopic composition of methane and other natural gases also indicates that even microbial methane has a  $\delta^{13}\text{C}_{\text{VPDB}}$  of  $-50\text{‰}$  (Milkov and Etiope, 2018). In this case, microbial methane could also be a carbon source for the AOM calcite.

Calcites formed where the DIC is derived from AOM as the carbonate source are generally depleted in  $^{13}\text{C}$ , with  $-125\text{‰}$  being the most negative  $\delta^{13}\text{C}_{\text{VPDB}}$  value reported from crystalline basement rocks (Drake et al., 2015). However, the  $\delta^{13}\text{C}$  of the AOM calcite would be influenced by several factors such as  $\delta^{13}\text{C}$  of the initial methane, the carbon-isotope fractionation, the ratio of oxidized to residual methane, and mixing proportions with DIC from other sources in the groundwater (Machel et al., 1995; Whiticar, 1999). For example, studies of fracture-filling calcite in the Fennoscandian shield have shown that the relatively higher  $\delta^{13}\text{C}$  of the AOM calcite found at Forsmark compared to other sites is due to the oxidation of methane derived from both methane of microbial origin, and methane produced by the thermogenic breakdown of organic matter (Drake et al., 2017). In the Mizunami area, two methane sources with different  $\delta^{13}\text{C}$  are present, and therefore there is the potential for a process whereby they are mixed and subsequently

oxidized. This study has identified two methane sources with different isotopic compositions as potential methane sources for the AOM calcite. However, it is difficult to define the methane source of the AOM calcite. Although the current AOM in the granitic groundwater may depend on sulfate ions supplied from sedimentary rocks and methane provided from greater depth (Fig. 5b) (Ino et al., 2018), sufficient evidence has not been obtained to fully-discuss the detailed process of past AOM. Further investigations are needed to determine past AOM processes in the Mizunami area.

The methanogenesis calcite was found to have occurred in a slightly deeper part of the sequence. Methanogenesis in present-day groundwater may utilize  $\text{H}_2$  supplied from greater depth (Ino et al., 2018). Since the potential for methanogenesis by other processes appears to be small, the same process may have occurred in the past.

The schematic diagram showing the occurrence of AOM and methanogenesis calcite is presented in Fig. 6. The AOM calcite and the methanogenic calcite in the Mizunami area were formed by mixing of meteoric water and seawater. The AOM calcite formed in the UHFD area with high fracture density and high permeability during the deposition of the organic-rich Toki Lignite-bearing Formation (Fig. 6 (a)). Consequently, methanogenesis calcite was found to have occurred in the same and/or slightly deeper area (Fig. 6 (b)). However, the methane source for the AOM is uncertain.

#### 4.4. Comparison of isotopic compositions with those in other sites

To compare the isotopic composition of calcite in the Toki granite that is presented in this study with the results of previous studies, we compile and plot the isotopic composition of calcite in crystalline rocks from Sweden (Drake et al., 2012, 2014, 2015, 2017; Drake and Tullborg, 2009; Fritz et al., 1989; Larson and Tullborg, 1984; Sandström and Tullborg, 2009; Tullborg et al., 1999; Tullborg, 1989; Tullborg and Larson, 1983; Wallin and Peterman, 1999), Finland (Blyth et al., 1998; Sahlstedt et al., 2010, 2013, 2014; Sahlstedt and Karhu, 2016), UK (spot

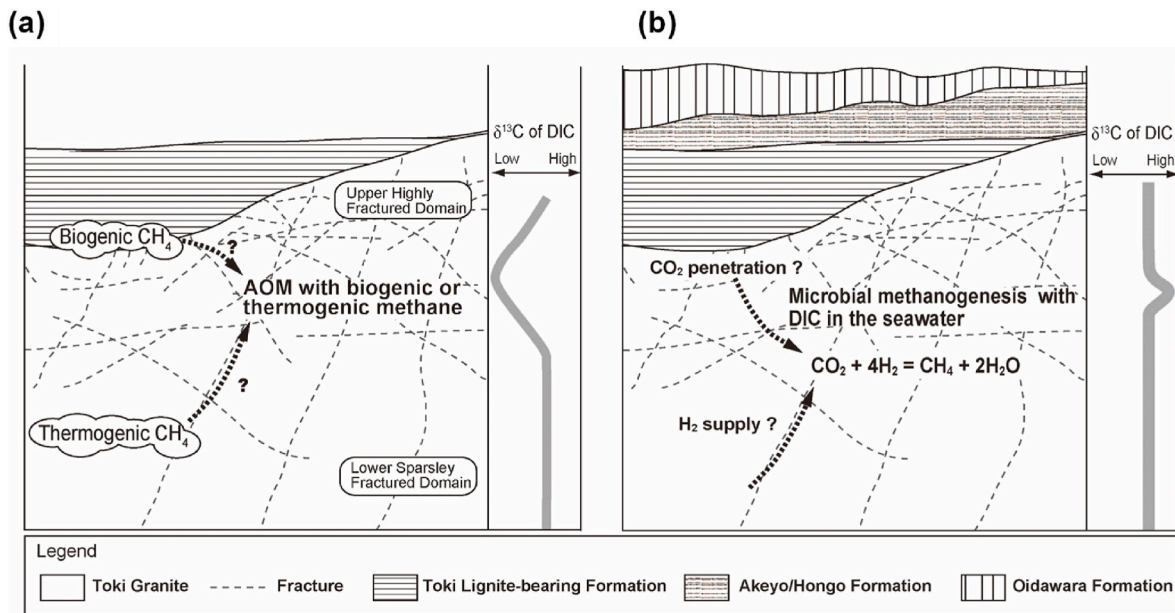


**Fig. 6.** Schematic illustration of possible (a) AOM and (b) methanogenesis processes in the past. The AOM calcite formed in the UHFD during the deposition of the Toki Lignite-bearing Formation. Then, Methanogenesis may have occurred in the same and/or slightly deeper area.

analysis) (Milodowski et al., 2018) and France (bulk-analysis) (Fourcade et al., 2002) (Fig. 7). The “bulk” sample and microsampled “point” analysis results are plotted separately in Fig. 7. Note that the UK data

includes the isotopic composition of calcite in sedimentary rocks. Because the study conducted at the Olkiluoto site yields results where only the carbon isotopic composition is analyzed, its  $\delta^{13}C_{VPDB}$  range is

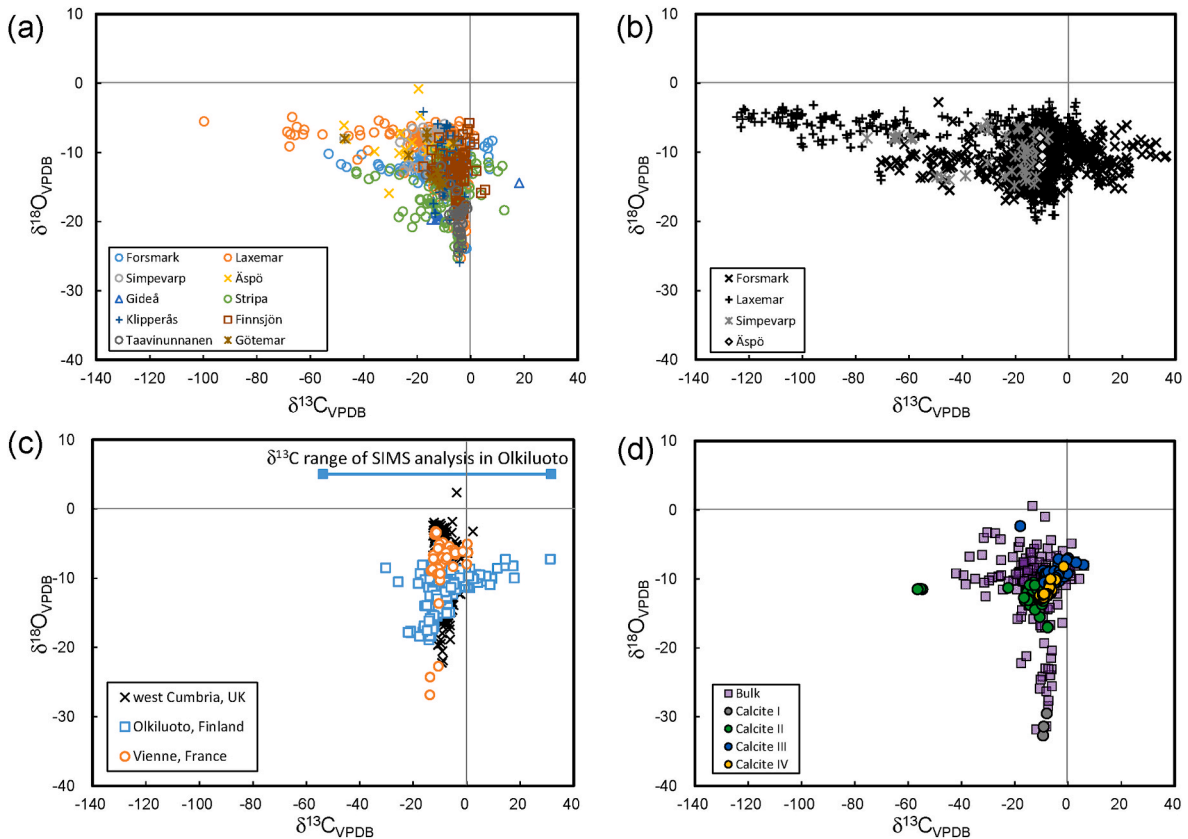


**Fig. 7.** Compiled  $\delta^{13}C_{VPDB}$  and  $\delta^{18}O_{VPDB}$  of fracture-filling calcite sampled from various fractured crystalline and basement rock sites: (a) Swedish sites with bulk analysis (Drake et al., 2015a, 2014, 2012; Drake and Tullborg, 2009; Fritz et al., 1989; Larson and Tullborg, 1984; Sandström and Tullborg, 2009; Tullborg et al., 1999; Tullborg, 1989; Tullborg and Larson, 1983; Wallin and Peterman, 1999); (b) Swedish sites with micro analysis (Drake et al., 2017a); (c) Finnish sites (Blyth et al., 1998; Sahlstedt et al., 2010, 2013, 2014; Sahlstedt and Karhu, 2016), west Cumbria, UK (Milodowski et al., 2018) and Vienne, France (Fourcade et al., 2002), and (d) Mizunami site, Japan.

indicated by the bar (Fig. 7c).

A review of isotopic data for fracture-filling calcite in crystalline rock indicates that there are common chemical controls on precipitation based on the similarity of isotopic compositional distributions at each site (Blyth et al., 2009). The review suggested that calcite with depleted  $^{18}\text{O}$  precipitated in hydrothermal environments, and calcite with  $\delta^{18}\text{O}_{\text{VPDB}}$  between  $-5\%$  and  $-20\%$  precipitated from meteoric or sea water with varying degrees of water-rock reaction (Blyth et al., 2009). It has also been shown that the very low  $\delta^{13}\text{C}$  in calcite originates from carbon due to AOM (Drake et al., 2015, 2017; Sahlstedt et al., 2016), while calcite with heavier isotopic compositions is precipitated from residual  $\text{CO}_2$  after methanogenesis as a carbon source (e.g., Drake et al., 2017; Sahlstedt et al., 2016; Sandström and Tullborg, 2009). The data compilation performed in this study (Fig. 7) also shows that the calcite at each Swedish site plots predominantly in areas presumed to have been precipitated from groundwater of freshwater or seawater origin. Calcite precipitated in hydrothermal environments is also present (Fig. 7a and b). The carbon isotopic ratio values also span a wide range due to methanogenesis and AOM (Fig. 7a and b). The analytical results of the calcite from Olkiluoto, while not as extreme as the Swedish results, similarly show a broad distribution of oxygen and carbon isotopic compositions from the calcite formation associated with hydrothermal fluids and methane (Fig. 7c). Although the isotopic composition of the calcite collected from the Vienne site in France appears to be less influenced by methane, the influence of the meteoric water, surface water, seawater, and even hydrothermal water can be confirmed as the origin of the groundwater, similar to that in the other sites (Fig. 7c). The distribution of isotopic compositions in the Mizunami area is comparable with those of these sites (Fig. 7d). This suggests that the hydrochemical conditions related to calcite precipitation at the Mizunami are similar to those at other crystalline sites.

## 5. Conclusion

In this study, carbon and oxygen stable isotopic analysis were undertaken on both bulk samples of calcite and spatially-resolved micro-samples of discrete generations of calcite within zoned crystals collected from calcite-mineralized fractures in the Toki granite in the Mizunami area in central Japan. The wide range of  $\delta^{18}\text{O}_{\text{VPDB}}$  exhibited by the fracture-filling calcite ( $-32.7\%$  to  $-0.59\%$ ) reflects the isotopic composition of residual warm hydrothermal fluids, infiltrating meteoric water and seawater, which are the origin of groundwater from which calcite precipitated. Although each of these groundwater types were present at different periods (Table 1), most of the calcite data suggests that they precipitated from a mixture of the groundwaters (Fig. 3). The  $\delta^{13}\text{C}_{\text{VPDB}}$  also shows a wide range (from  $-56.6\%$  to  $+6.0\%$ ). The  $\delta^{13}\text{C}_{\text{VPDB}}$  ranging from  $-16.2\%$  to  $+2.8\%$  suggested that the major carbon sources were soil  $\text{CO}_2$  supplied from the surface, DIC from organic matter degradation in the overlying organic-rich sedimentary strata, and DIC in seawater. However, many samples exhibit  $\delta^{13}\text{C}_{\text{VPDB}}$  values outside that range. The calcite with more negative  $\delta^{13}\text{C}_{\text{VPDB}}$  than  $-25\%$  was interpreted to have precipitated by AOM, and calcite with  $\delta^{13}\text{C}_{\text{VPDB}}$  above  $+2.8\%$  inferred to have precipitated from groundwater with residual DIC of methanogens.

The distribution of AOM calcite in the Mizunami area is only found in the UHFD, which has a high fracture density, and active mass transportation from shallow depth is expected. The methane involved in AOM was assumed to be either the methane with very low  $\delta^{13}\text{C}_{\text{VPDB}}$  ( $-97\%$ ) identified at the Tono uranium mine, or the methane dissolved in the present-day granitic groundwater with more positive  $\delta^{13}\text{C}_{\text{VPDB}}$  ( $-46.3\%$  to  $-21.0\%$ ). However, the precise source of methane could not be identified from the results of this study. Methanogenesis calcite was found to have occurred in the same and/or slightly deeper regions. Further investigations are needed to determine the detailed process of AOM and methanogenesis in the Toki Granite.

These results indicate that AOM also occurs in crystalline rocks in

areas other than that previously reported from crystalline rocks in stable crustal regions, and that AOM may occur in a wide geological environment. Understanding the carbon cycle in these environments is an important insight into assessing the long-term safety of geological-disposal systems for high-level radioactive waste.

## Author contributions

All authors contributed to the study conception and design. Sampling of materials was performed by Takashi Mizuno and Antoni Edward Milodowski. Mineralogical observation and isotopic data collection were performed by Antoni Edward Milodowski and Teruki Iwatsuki. The first draft of the manuscript was written by Takashi Mizuno and all authors commented on previous versions of the manuscript. All authors read and approved the final manuscript.

## Declaration of competing interest

The authors declare that they have no known competing financial interests or personal relationships that could have appeared to influence the work reported in this paper.

## Data availability

Data will be made available on request.

## Acknowledgments

Constructive reviews by two anonymous reviewers were very helpful in revising the manuscript. The authors also thank Y. Amano (JAEA) for improving the manuscript. AEM publishes with the permission of the Director of the British Geological Survey, part of United Kingdom Research and Innovation (UKRI).

## Appendix A. Supplementary data

Supplementary data to this article can be found online at <https://doi.org/10.1016/j.apgeochem.2023.105571>.

## References

- Alperin, M.J., Reeburgh, W.S., Whiticar, M.J., 1988. Carbon and hydrogen isotope fractionation resulting from anaerobic methane oxidation. *Global Biogeochem. Cycles* 2, 279–288. <https://doi.org/10.1029/GB002i003p00279>.
- Bath, A., Milodowski, A., Ruotsalainen, P., Tullborg, E., Cortés Ruiz, A., Aranyosy, J.F., 2000. Evidence from Mineralogy and Geochemistry for the Evolution of Groundwater Systems during the Quaternary for Use in Radioactive Waste Repository Safety Assessment (EQUIP Project). EUR(Luxembourg). <https://doi.org/10.13140/RG.2.1.3067.1848>.
- Blyth, A., Frapé, S., Blomqvist, R., Nissinen, P., McNutt, R., 1998. An Isotopic and Fluid Inclusion Study of Fracture Calcite from Borehole OL-KR1 at the Olkiluoto Site. POSIVA, Finland, 98–04.
- Blyth, A.R., Frapé, S.K., Tullborg, E.-L., 2009. A review and comparison of fracture mineral investigations and their application to radioactive waste disposal. *Appl. Geochem.* 24, 821–835. <https://doi.org/10.1016/j.apgeochem.2008.12.036>.
- Bombard, M., Nyyssönen, M., Pitkänen, P., Lehtinen, A., Itävaara, M., 2015. Active microbial communities inhabit sulphate-methane interphase in deep bedrock fracture fluids in Olkiluoto. Finland. *Biomed. Res. Int.* <https://doi.org/10.1155/2015/979530>, 2015.
- Bottinga, Y., 1968. Calculation of fractionation factors for carbon and oxygen isotopic exchange in the system calcite-carbon dioxide-water. *J. Phys. Chem.* 72, 800–808. <https://doi.org/10.1021/j100849a008>.
- Chanton, J.P., Powelson, D.K., Abichou, T., Fields, D., Green, R., 2008. Effect of temperature and oxidation rate on carbon-isotope fractionation during methane oxidation by landfill cover materials. *Environ. Sci. Technol.* 42, 7818–7823. <https://doi.org/10.1021/es801221y>.
- Clark, I.D., Fritz, P., 1997. *Environmental Isotopes in Hydrogeology*. CRC Press.
- Degnan, P., Bath, A., Cortés, A., Delgado, J., Haszeldine, S., Milodowski, A., Puigdomenech, I., Recreo, F., Silar, J., Torres, T., Tullborg, E.-L., 2005. Padamot : project overview report. PADAMOT Proj. Tech. Rep.
- Douglas, P.M.J., Stolper, D.A., Eiler, J.M., Sessions, A.L., Lawson, M., Shuai, Y., Bishop, A., Podlaha, O.G., Ferreira, A.A., Santos Neto, E.V., Niemann, M., Steen, A.S., Huang, L., Chimiak, L., Valentine, D.L., Fiebig, J., Luhmann, A.J., Seyfried, W.E.,

- Etiopie, G., Schoell, M., Inskip, W.P., Moran, J.J., Kitchen, N., 2017. Methane clumped isotopes: progress and potential for a new isotopic tracer. *Org. Geochem.* 113, 262–282. <https://doi.org/10.1016/j.orggeochem.2017.07.016>.
- Drake, H., Tullborg, E.-L., 2009. Paleohydrogeological events recorded by stable isotopes, fluid inclusions and trace elements in fracture minerals in crystalline rock, Simpevarp area, SE Sweden. *Appl. Geochem.* 24, 715–732. <https://doi.org/10.1016/j.apgeochem.2008.12.026>.
- Drake, H., Tullborg, E.-L., Hogmalm, K.J., Åström, M.E., 2012. Trace metal distribution and isotope variations in low-temperature calcite and groundwater in granitoid fractures down to 1 km depth. *Geochem. Cosmochim. Acta* 84, 217–238. <https://doi.org/10.1016/j.gca.2012.01.039>.
- Drake, H., Heim, C., Hogmalm, K.J., Hansen, B.T., 2014. Fracture zone-scale variation of trace elements and stable isotopes in calcite in a crystalline rock setting. *Appl. Geochem.* 40, 11–24. <https://doi.org/10.1016/j.apgeochem.2013.10.008>.
- Drake, H., Åström, M.E., Heim, C., Broman, C., Åström, J., Whitehouse, M., Ivarsson, M., Siljeström, S., Sjövall, P., 2015. Extreme  $^{13}\text{C}$  depletion of carbonates formed during oxidation of biogenic methane in fractured granite. *Nat. Commun.* 6, 7020. <https://doi.org/10.1038/ncomms8020>.
- Drake, H., Heim, C., Roberts, N.M.W., Zack, T., Tillberg, M., Broman, C., Ivarsson, M., Whitehouse, M.J., Åström, M.E., 2017. Isotopic evidence for microbial production and consumption of methane in the upper continental crust throughout the Phanerozoic eon. *Earth Planet Sci. Lett.* 470, 108–118. <https://doi.org/10.1016/j.epsl.2017.04.034>.
- Drake, H., Ivarsson, M., Tillberg, M., Whitehouse, M.J., Kooijman, E., 2018. Ancient Microbial Activity in Deep Hydraulically Conductive Fracture Zones within the Forsmark Target Area for Geological Nuclear Waste Disposal, vol. 8. Geosci. Sweden. <https://doi.org/10.33390/geosciences8060211>.
- Fourcade, S., Michelot, J.L., Buschaert, S., Cathelineau, M., Freiberger, R., Coulbaly, Y., Aranyosy, J.F., 2002. Fluid transfers at the basement/cover interface Part I. Subsurface recycling of trace carbonate from granitoid basement rocks (France). *Chem. Geol.* 192, 99–119. [https://doi.org/10.1016/S0009-2541\(02\)00192-4](https://doi.org/10.1016/S0009-2541(02)00192-4).
- Fritz, P., Fontes, J.C., Frapé, S.K., Louvat, D., Michelot, J.L., Balderer, W., 1989. The isotope geochemistry of carbon in groundwater at Stripa. *Geochem. Cosmochim. Acta* 53, 1765–1775. [https://doi.org/10.1016/0016-7037\(89\)90297-4](https://doi.org/10.1016/0016-7037(89)90297-4).
- Fukuda, A., Hagiwara, H., Ishimura, T., Kouduka, M., Ioka, S., Amano, Y., Tsunogai, U., Suzuki, Y., Mizuno, T., 2010. Geomicrobiological properties of ultra-deep granitic groundwater from the Mizunami underground research laboratory (MIU), central Japan. *Microb. Ecol.* 60, 214–225. <https://doi.org/10.1007/s00248-010-9683-9>.
- Gilg, H.A., Krüger, Y., Taubald, H., van den Kerkhof, A.M., Frenz, M., Morteani, G., 2014. Mineralisation of amethyst-bearing geodes in Ametista do Sul (Brazil) from low-temperature sedimentary brines: evidence from monophase liquid inclusions and stable isotopes. *Miner. Deposits* 49, 861–877. <https://doi.org/10.1007/s00126-014-0522-7>.
- Hiroki, Y., Matsumoto, R., 1999. Magnetostratigraphic correlation of Miocene regression-and-transgression boundaries in central Japan. *J. Geol. Soc. Japan* 105, 81–107. <https://doi.org/10.1248/cpb.37.3229>.
- IAEA, 2012. The Safety Case and Safety Assessment for the Disposal of Radioactive Waste. IAEA Saf. Stand. Ser. Specif. Saf. Guid. No. SSG-23 140.
- Ino, K., Hemsdorf, A.W., Konno, U., Kouduka, M., Yanagawa, K., Kato, S., Sunamura, M., Hirota, A., Togo, Y.S., Ito, K., Fukuda, A., Iwatsuki, T., Mizuno, T., Komatsu, D.D., Tsunogai, U., Ishimura, T., Amano, Y., Thomas, B.C., Banfield, J.F., Suzuki, Y., 2018. Ecological and genomic profiling of anaerobic methane-oxidizing archaea in a deep granitic environment. *ISME J.* 12, 31–47. <https://doi.org/10.1038/ismej.2017.140>.
- Ishibashi, M., Yoshida, H., Sasao, E., Yuguchi, T., 2016. Long term behavior of hydrogeological structures associated with faulting: an example from the deep crystalline rock in the Mizunami URL, Central Japan. *Eng. Geol.* 208, 114–127. <https://doi.org/10.1016/j.enggeo.2016.04.026>.
- Iwatsuki, T., Yoshida, H., 1999. Groundwater chemistry and fracture mineralogy in the basement granitic rock in the Tono uranium mine area, Gifu Prefecture, Japan—groundwater composition, Eh evolution analysis by fracture filling mineral. *Geochem. J.* 33.
- Iwatsuki, T., Sato, K., Seo, T., Hama, K., 1995. Hydrogeochemical investigation of groundwater in the Tono area, Japan. *Proc. Mat. Res. Soc. Symp.* 353, 1251–1257.
- Iwatsuki, T., Xu, S., Mizutani, Y., Hama, K., Saegusa, H., Nakano, K., 2001. Carbon-14 study of groundwater in the sedimentary rocks at the Tono study site, central Japan. *Appl. Geochem.* 16, 849–859.
- Iwatsuki, T., Satake, H., Metcalfe, R., Yoshida, H., Hama, K., 2002. Isotopic and morphological features of fracture calcite from granitic rocks of the Tono area, Japan: a promising palaeohydrogeological tool. *Appl. Geochem.* 17, 1241–1257.
- Iwatsuki, T., Arthur, R., Ota, K., Metcalfe, R., 2004. Solubility constraints on uranium concentrations in groundwaters of the Tono uranium deposit, Japan. *Radiochim. Acta* 92, 789–796. <https://doi.org/10.1524/ract.92.9.789.54986>.
- Iwatsuki, T., Furue, R., Mie, H., Ioka, S., Mizuno, T., 2005. Hydrochemical baseline condition of groundwater at the Mizunami underground research laboratory (MIU). *Appl. Geochem.* 20, 2283–2302. <https://doi.org/10.1016/j.apgeochem.2005.09.002>.
- Iwatsuki, T., Mizuno, T., Hama, K., Kunimaru, T., 2010. Mineralogical analysis of a long-term groundwater system in Tono and Horonobe area, Japan. In: Taniguchi, M., Holman, I.P. (Eds.), *Groundwater Response to Changing Climate*. CRC Press, pp. 87–98. <https://doi.org/10.1201/b10530>.
- Judd, A.G., Hovland, M., 2007. *Seabed Fluid Flow: the Impact of Geology, Biology and the Marine Environment*. Cambridge University Press, United Kingdom.
- Judd, A., Noble-James, T., Golding, N., Eggett, A., Dising, M., Clare, D., Silburn, B., Duncan, G., Field, L., Milodowski, A., 2019. The Croker Carbonate Slabs: extensive methane-derived authigenic carbonate in the Irish Sea—nature, origin, longevity and environmental significance. *Geo Mar. Lett.* <https://doi.org/10.1007/s00367-019-00584-0>.
- Kuivila, K.M., Murray, J.W., Devol, A.H., Novelli, P.C., 1989. Methane production, sulfate reduction and competition for substrates in the sediments of Lake Washington. *Geochem. Cosmochim. Acta* 53, 409–416. [https://doi.org/10.1016/0016-7037\(89\)90392-X](https://doi.org/10.1016/0016-7037(89)90392-X).
- Kurosawa, H., Niwa, M., Ishimaru, T., Shimada, K., 2010. Study on Method of Fault Zone Survey by Use of In-Situ Fault Gas ( $\text{H}_2$ ,  $\text{CO}_2$ ,  $\text{CH}_4$ ) Measurement (Measurement Data Set), vol. 36. JAEA-Data/Code, 2010.
- Larson, S.A., Tullborg, E.-L., 1984. Fracture fillings in the gabbro massif of Taavannanen, northern Sweden. SKB/KBS Tech. Rep. 84–08.
- Machel, H.G., Krouse, H.R., Sassen, R., Watkin, L., 1995. Products and distinguishing criteria of bacterial and thermochemical sulfate reduction. *Appl. Geochem.* 10, 373–389. [https://doi.org/10.1016/0883-2927\(95\)00008-8](https://doi.org/10.1016/0883-2927(95)00008-8).
- Milkov, A.V., Etiopie, G., 2018. Revised genetic diagrams for natural gases based on a global dataset of >20,000 samples. *Org. Geochem.* 125, 109–120. <https://doi.org/10.1016/j.orggeochem.2018.09.002>.
- Mills, C.T., Amano, Y., Slater, G.F., Dias, R.F., Iwatsuki, T., Mandernack, K.W., 2010. Microbial carbon cycling in oligotrophic regional aquifers near the Tono Uranium Mine, Japan as inferred from  $\delta^{13}\text{C}$  and  $\Delta^{14}\text{C}$  values of in situ phospholipid fatty acids and carbon sources. *Geochem. Cosmochim. Acta* 74, 3785–3805. <https://doi.org/10.1016/j.gca.2010.03.016>.
- Milodowski, A.E., Tullborg, E.-L., Buil, B., Gómez, P., Turrero, M.J., Haszeldine, S., E, G., Gillespie, M.R., Torres, T., Ortiz, J.E., Zachariás, J., Silar, J., Chvátal, A.L.M., Strnad, L., Sebek, O., Bouch, J.E., Chenery, S.R., Chenery, C., Shepherd, T.J., McKevey, J.A., 2005. Application of Mineralogical, Petrological and Geochemical Tools for Evaluating the Palaeohydrogeological Evolution of the PADAMOT Study Sites.
- Milodowski, A.E., Bath, A., Norris, S., 2018. Palaeohydrogeology using geochemical, isotopic and mineralogical analyses: salinity and redox evolution in a deep groundwater system through Quaternary glacial cycles. *Appl. Geochem.* 97, 40–60. <https://doi.org/10.1016/j.apgeochem.2018.07.008>.
- Mizuno, T., Milodowski, A.E., Iwatsuki, T., 2010. Evaluation of the long-term evolution of the groundwater system in the Mizunami area, Japan. In: ASME 2010 13th International Conference on Environmental Remediation and Radioactive Waste Management, vol. 2. ASME, pp. 193–201. <https://doi.org/10.1115/ICEM2010-40070>.
- Mizuno, T., Milodowski, A.E., Iwatsuki, T., 2022. Precipitation sequence of fracture-filling calcite in fractured granite and changes in the fractionation process of rare earth elements and yttrium. *Chem. Geol.* 603, 120880. <https://doi.org/10.1016/j.chemgeo.2022.120880>.
- Mizutani, Y., Seo, T., K, O., Nakai, N., Murai, Y., 1992. Carbon-14 ages of deep groundwater from the Tono uranium mine, Gifu, Japan. *Proc. Symp. Accel. Mass Spectrom. Interdiscip. Appl. Carbon Isot* 159–168.
- Mook, W.G., Bommerson, J.C., Staverman, W.H., 1974. Carbon isotope fractionation between dissolved bicarbonate and gaseous carbon dioxide. *Earth Planet Sci. Lett.* 22, 169–176.
- Niwa, M., Amano, K., Takeuchi, R., Shimada, K., 2021. Rapid identification of water-conducting fractures using a trace methane gas measurement. *Groundw. Monit. Remediat.* 1–10. <https://doi.org/10.1111/gwmr.12428>.
- OECD/NEA, 2013. *The Nature and Purpose of the Post-closure Safety Cases for Geological Repositories NEA/RWM/R(2013)1*.
- Oy, Posiva, 2012. Safety case for the disposal of spent nuclear fuel at Olkiluoto - synthesis 2012. *Posiva Rep* 12, 2012.
- O'Neil, J.R., Clayton, R.N., Mayeda, T.K., 1969. Oxygen isotope fractionation in divalent metal carbonates. *J. Chem. Phys.* 51, 5547–5558. <https://doi.org/10.1063/1.1671982>.
- Phelps, T.J., Zeikus, J.G., 1985. Effect of fall turnover on terminal carbon metabolism in lake mendota sediments. *Appl. Environ. Microbiol.* 50, 1285–1291. <https://doi.org/10.1128/aem.50.5.1285-1291.1985>.
- Roedder, E., 1984. *Fluid Inclusions, Reviews in Mineralogical Society of America*, Washington D.C.
- Saegusa, H., Matsuoka, T. (Eds.), 2011. *Final Report on the Surface-Based Investigation Phase (Phase I) at the Mizunami Underground Research Laboratory Project*. Japan Atomic Energy Agency. JAEA-Research 2010-067.
- Sahlstedt, E., Karhu, J., 2016. Mineralogical, stable isotope and fluid inclusion studies of fracture filling calcite at hästholmen, syrry and Olkiluoto. *POSIVA Work. Rep.* 35, 2016.
- Sahlstedt, E., Karhu, J.A., Pitkanen, P., 2010. Indications for the past redox environments in deep groundwaters from the isotopic composition of carbon and oxygen in fracture calcite, Olkiluoto, SW Finland. *Isot. Environ. Health Stud.* 46, 370–391. <https://doi.org/10.1080/10256016.2010.505981>.
- Sahlstedt, E., Karhu, J.A., Pitkanen, P., Whitehouse, M., 2013. Implications of sulfur isotope fractionation in fracture-filling sulfides in crystalline bedrock, Olkiluoto, Finland. *Appl. Geochem.* 32, 52–69. <https://doi.org/10.1016/j.apgeochem.2012.10.021>.
- Sahlstedt, E., Karhu, J., Rinne, K., 2014. Fracture mineral investigations at Olkiluoto in 2010: implications to paleohydrogeology. *POSIVA Work. Rep.* 94, 2012.
- Sahlstedt, E., Karhu, J.A., Pitkanen, P., Whitehouse, M., 2016. Biogenic processes in crystalline bedrock fractures indicated by carbon isotope signatures of secondary calcite. *Appl. Geochem.* 67, 30–41. <https://doi.org/10.1016/j.apgeochem.2016.01.010>.
- Sakai, H., Matsubaya, O., 1974. Isotopic geochemistry of the thermal waters of Japan and its bearing on the kuroko ore solutions. *Econ. Geol.* 69, 974–991. <https://doi.org/10.2113/gsecongeo.69.6.974>.

- Sandström, B., Tullborg, E.-L., 2009. Episodic fluid migration in the Fennoscandian Shield recorded by stable isotopes, rare earth elements and fluid inclusions in fracture minerals at Forsmark, Sweden. *Chem. Geol.* 266, 126–142. <https://doi.org/10.1016/j.chemgeo.2009.04.019>.
- Sasao, E., 2013. Petrographic study of the miocene Mizunami group, Central Japan: detection of unrecognized volcanic activity in the setouchi province. *Isl. Arc* 22, 170–184. <https://doi.org/10.1111/iar.12019>.
- Sasao, E., Kenji, A., Kunio, O., 2005. Natural analogue study in the Tono uranium deposit - quantitative estimation of uplift and subsidence, and vertical displacement rate - in Japanese. *J. Nucl. Fuel Cycle Environ.* 11.
- Sasao, E., Ota, K., Iwatsuki, T., Niizato, T., Arthur, R.C., Stenhouse, M.J., Zhou, W., Metcalfe, R., Takase, H., Mackenzie, A.B., 2006. An overview of a natural analogue study of the Tono Uranium Deposit, central Japan. *Geochem. Explor. Environ. Anal.* <https://doi.org/10.1144/1467-7873/05-084>.
- Schoell, M., 1980. The hydrogen and carbon isotopic composition of methane from natural gases of various origins. *Geochem. Cosmochim. Acta* 44, 649–661. [https://doi.org/10.1016/0016-7037\(80\)90155-6](https://doi.org/10.1016/0016-7037(80)90155-6).
- Shibata, K., Ishihara, S., 1979. Rb-Sr whole-rock of granitic rocks in Japan. *Geochem. J.* 13, 113–119.
- Shikazono, N., Utada, M., 1997. Stable isotope geochemistry and diagenetic mineralization associated with the Tono sandstone-type uranium deposit in Japan. *Miner. Deposits* 32, 596–606. <https://doi.org/10.1007/s001260050125>.
- SKB, 2011. Long-term Safety for the Final Repository for Spent Nuclear Fuel at Forsmark Main Report of the SR-Site Project. *Tech. Rep. TR-11-01*.
- Stumm, W., Morgan, J.J., 1996. *Aquatic Chemistry: Chemical Equilibria and Rates in Natural Waters*, third ed. ed. John Wiley & Sons, New York.
- Suzuki, Y., Konno, U., Fukuda, A., Komatsu, D.D., Hirota, A., Watanabe, K., Togo, Y., Morikawa, N., Hagiwara, H., Aosai, D., Iwatsuki, T., Tsunogai, U., Nagao, S., Ito, K., Mizuno, T., 2014. Biogeochemical signals from deep microbial life in terrestrial crust. *PLoS One* 9, e113063. <https://doi.org/10.1371/journal.pone.0113063>.
- Tsuruta, T., Tagami, M., Amano, K., Matsuoka, T., Kurihara, A., Yamada, Y., Koike, K., 2013. Geological investigations for geological Model of deep underground geoenvironment at the Mizunami underground research laboratory (MIU). *J. Geol. Soc. Japan* 119, 59–74. <https://doi.org/10.5575/geosoc.2011.0010>.
- Tullborg, E.-L., 1989. The influence of recharge water on fissure-filling minerals - a study from Klipperås, southern Sweden. *Chem. Geol.* 76, 309–320. [https://doi.org/10.1016/0009-2541\(89\)90099-5](https://doi.org/10.1016/0009-2541(89)90099-5).
- Tullborg, E.-L., Larson, S.Å., 1983. Fissure fillings from gideå, central Sweden. *SKB Tech. Rep.* 83-74.
- Tullborg, E.-L., Landström, O., Wallin, B., 1999. Low-temperature trace element mobility influenced by microbial activity—indications from fracture calcite and pyrite in crystalline basement. *Chem. Geol.* 157, 199–218. [https://doi.org/10.1016/S0009-2541\(99\)00002-9](https://doi.org/10.1016/S0009-2541(99)00002-9).
- Tullborg, E.-L., Drake, H., Sandström, B., 2008. Palaeohydrogeology: a methodology based on fracture mineral studies. *Appl. Geochem.* 23, 1881–1897. <https://doi.org/10.1016/j.apgeochem.2008.02.009>.
- Wallin, B., Peterman, Z., 1999. Calcite fracture fillings as indicators of paleohydrology at laxemar at the aspo hard rock laboratory, southern Sweden. *Appl. Geochem.* 14, 953–962. [https://doi.org/10.1016/S0883-2927\(99\)00028-1](https://doi.org/10.1016/S0883-2927(99)00028-1).
- Whiticar, M.J., 1999. Carbon and hydrogen isotope systematics of bacterial formation and oxidation of methane. *Chem. Geol.* 161, 291–314. [https://doi.org/10.1016/S0009-2541\(99\)00092-3](https://doi.org/10.1016/S0009-2541(99)00092-3).
- Whiticar, M.J., Faber, E., Schoell, M., 1986. Biogenic methane formation in marine and freshwater environments: CO<sub>2</sub> reduction vs acetate fermentation - isotope evidence. *Geochem. Cosmochim. Acta* 50, 693–709. [https://doi.org/10.1016/0016-7037\(86\)90346-7](https://doi.org/10.1016/0016-7037(86)90346-7).
- Yamasaki, S., Zwingmann, H., Yamada, K., Tagami, T., Umeda, K., 2013. Constraining the timing of brittle deformation and faulting in the Toki granite, central Japan. *Chem. Geol.* 351, 168–174. <https://doi.org/10.1016/j.chemgeo.2013.05.005>.
- Yuguchi, T., Sueoka, S., Iwano, H., Izumino, Y., Ishibashi, M., Danhara, T., Sasao, E., Hirata, T., Nishiyama, T., 2019. Position-by-position cooling paths within the Toki granite, central Japan: constraints and the relation with fracture population in a pluton. *J. Asian Earth Sci.* 169, 47–66. <https://doi.org/10.1016/j.jseaes.2018.07.039>.
- Yuguchi, T., Izumino, Y., Sasao, E., 2021. Genesis and development processes of fractures in granite: petrographic indicators of hydrothermal alteration. *PLoS One* 16, 1–17. <https://doi.org/10.1371/journal.pone.0251198>.